INFLUENCE OF CRYOGENIC TREATMENTS ON THE ELECTROCHEMICAL BEHAVIOR OF TWO MARTENSITIC STAINLESS STEELS

D. FLAMINI [1,2], *W. R. TUCKART* [3,4], *G. PRIETO* [3,4]

[1] *Instituto de Ingeniería Electroquímica y Corrosión – INIEC, Departamento de Ingeniería Química, Universidad Nacional del Sur, Bahía Blanca, Buenos Aires, Argentina;*

[2] *CONICET, Ciudad Autónoma de Buenos Aires, Argentina;*

[3] *IFISUR, Bahía Blanca, Buenos Aires, Argentina;*

[4] *Departamento de Ingeniería, Universidad Nacional del Sur, Bahía Blanca, Buenos Aires, Argentina*

Cryogenic treatment is a useful method for improving the mechanical and tribological properties of a wide range of materials, especially steels. However, results regarding the effect of this treatment on the corrosion resistance are scarce, particularly in the case of martensitic stainless steels. In this research, the influence of cryogenic treatments on the properties of two different martensitic stainless steels, namely AISI 420 and AISI 440C, is investigated. Their microstructures are studied by scanning electron microscopy and X-ray diffraction and correlated with their corrosion resistance. The electrochemical behavior of the steels is studied by measuring open-circuit potential and under experiments using cyclic anodic potentiodynamic polarization. It is found that the cryogenic treatment does not affect the pitting resistance of AISI 420 steel, but it significantly reduces the ability of AISI 440C to achieve passivation.

Keywords: *cryogenic treatment, electrochemical corrosion, carbides, retained austenite.*

Кріогенне оброблення використовують для підвищення механічних і трибологічних характеристик багатьох матеріалів, зокрема сталей. Однак його вплив на корозійну тривкість мартенситних нержавних сталей вивчено недостатньо. Більше уваги приділяли мартенситним нержавним сталям AISI 420 та AISI 440. Їх мікроструктуру проаналізовано з допомогою сканівної електронної мікроскопії та методу рентгенівської спектроскопії. Електрохімічні властивості вивчено за вільного потенціалу корозії та циклічної анодної потенціодинамічної поляризації. Виявлено, що кріогенне оброблення не змінює тривкості до пітингоутворення сталі AISI 420, але значно знижує здатність до пасивації сталі AISI 440.

Ключові слова: *кріогенне оброблення, електрохімічна корозія, карбіди, залишковий аустеніт.*

Introduction. Martensitic stainless steels are designed for obtaining a balance between their mechanical properties and corrosion resistance. Their high levels of ultimate strength and yield stress are caused by the martensitic phase, while the addition of chromium content above 12 wt.% provides them with adequate resistance to mildly corrosive environments.

In the present study, two different martensitic stainless steels are investigated: AISI 420 and AISI 440C. The first of them is used in pumping applications in the petrochemical industry, oil extraction, and energy generation. Due to its chemical composition, this steel is characterized by high hardenability and a low retained austenite content after quenching. The hardness of the AISI 440C steel can reach values up to 60 HRC and yield stresses in the range of 1900 MPa. It is used in bearings, pumps, valves, and

Corresponding authors: G. PRIETO, e-mail: german.prieto@uns.edu.ar

aircraft components. Both steels can be in contact with fresh water, organic materials, and petrochemical products.

In addition to the conventional heat treatments of these steels, their mechanical properties can be enhanced with the application of deep cryogenic treatments (DCT), which assume the cooling of the samples well below room temperature. This cooling stage is usually carried out in liquid nitrogen at –196°C immediately after completion of the quenching stage and before the tempering. Cryogenic treatments can enhance the mechanical and tribological properties of a wide range of materials, including tool steels [1–4], martensitic stainless steels [5–7], non-ferrous alloys [8–10] and even non-metallic materials [11].

In the particular case of steels, the main mechanisms responsible for these improvements are the reduction of the amount of retained austenite and the refinement of the carbide precipitates [12]. It is expected that these microstructural modifications also affect the corrosion behavior of the steels. In this sense, the authors of [15] have reported that the structural heterogeneity of the steel can decrease the corrosion resistance of the 20Kh13 martensitic stainless steel, due to local variations in the chromium content. It should be noted that there is the only study [16] addressing the corrosion behavior of a cryogenically treated martensitic stainless steel that could be found in the open literature. The authors have found no significant differences between the corrosion resistance of conventional and cryogenically treated AISI 420 steel. This result was attributed to the fact that both groups of specimens have the same amount of retained austenite.

The objective of this research work is to determine the influence of the microstructural modifications generated by the application of cryogenic treatments on the electrochemical behavior, namely the pitting and the passivation potentials of two martensitic stainless steels.

Materials and methods. In the present study, two martensitic stainless steels were used: AISI 420 and AISI 440C. Chemical compositions of these steels are determined using a spectromax optical emission spectrometer are as follows (wt.%): AISI 420 – 0.17 C; 12.83 Cr; 0.76 Mn; 0.55 Si; 0.05 P; 0.17 S; Fe – balance; AISI 440C – 1.10 C; 16.97 Cr; 0.36 Mn; 0.40 Si; 0.023 P; 0.0075 S; Fe – balance.

The samples were machined to prisms with 1 cm^2 square section and 10 mm in length. Every stage of the heat treatments (Table 1) was performed in an argon atmosphere furnace, to prevent the oxidation and decarburation of the samples.

Table 1. Applied heat treatments

Steel	Heat treatment	Identification
AISI 420	Austenitizing at 1030°C for 10 min, quenched in oil, tempered at 410°C for 10 min	420-CHT*
AISI 420	Austenitizing at 1030°C for 10 min, quenched in oil, hold in liquid nitrogen (–196°C) for 120 min, tempered at 410°C for 10 min	420-DCT*
AISI 440C	Austenitizing at 1055°C for 45 min, quenched in oil, tempered at 190°C for 120 min	440-CHT
AISI 440C	Austenitizing at 1055°C for 45 min, quenched in oil, hold in liquid nitrogen (–196°C) for 300 min, tempered at 190°C for 120 min	440-DCT

*CHT – conventional heat treatment; DCT – deep cryogenic treatment.

The samples were mechanically abraded using abrasive SiC papers down to 2500 grit finish and etched to reveal the microstructural features. The AISI 440C samples were etched with Vilella's reagent (1 g picric acid + 5 ml hydrochloric acid + 95 ml ethyl alcohol) by direct immersion for 10 min, while AISI 420 samples were etched with Marble's reagent (50 ml hydrochloric acid + 10 g $CuSO_4$ + 50 ml H_2O) for 20 s. The samples were examined using a scanning electron microscope (SEM) CARL ZEISS EVO MA10 equipped with a Cambridge X-ACT energy dispersion spectrometer (EDS) to evaluate the microstructure and the pitting damage after the corrosion tests.

SEM micrographs were processed using FIJI [17] for estimating the characteristics of the carbide precipitates and the amount of retained austenite. The reported values correspond to the average of at least three measurements for each group of specimens. This second characteristic was also evaluated using X-ray diffraction, performed with a Panalytical X'PERT-MPD diffractometer, using a CuK_α-radiation (λ = 1.5405 Å). The diffraction angle ranged from 20° to 120° with a 0.02° step. The hardness of the samples was measured after the heat treatments using a Future Tech FT-300 Vickers durometer with an applied test load of 500 grf. At least 30 measurements were taken for each group of specimens.

The electrochemical experiments were performed at room temperature using a PAR Model 237A potentiostat/galvanostat and SoftCorrTM II software. All electrochemical measurements were performed at least three times for each sample and the obtained values were reproducible. The reference electrode was a saturated calomel electrode (SCE), while the counter electrode was a 1 cm^2 platinum sheet. The electrolyte used in all the experiments was a naturally aerated 0.5 M NaCl solution (pH 6.5 ± 0.2) prepared with reagent grade NaCl (98%, Aldrich). The lateral surfaces of the samples were covered with an epoxy resin in such a way that only one of them with an area of 1 cm^2 was exposed to the electrolyte. The open-circuit potential (OCP) measurements were taken continuously for one hour to monitor the variation of its value during the immersion process.

Cyclic anodic potentiodynamic polarization curves with a scanning rate of 1 $mV \cdot s^{-1}$ were performed from –0.3 V (SCE) with respect to OCP, after a process stabilization of 1 h in the test solution, up to $5 \cdot 10^{-3}$ $A \cdot cm^{-2}$. Afterward, the scan was activated into the reverse direction to complete repassivation, indicated by the potential at which the anodic current density reached its lowest value.

Current versus time responses at a potential of 0.2 V (SCE) are used in order to analyze the influence of deep cryogenic and conventional heat treatments on the pitting corrosion resistance of the AISI 420 and AISI 440C martensitic stainless steels.

Results and discussion. ***Hardness and microstructural characterization*****.** The cryogenic treatments increased the hardness of the samples of both stainless steels. In the case of AISI 420 samples, the effect of the hardening after cryogenic treatment was rather negligible, with an increase of 4.6% in comparison to CHT samples [5], while the hardness of cryogenically treated AISI 440C samples increases by 7.8%. The level of hardness increase in AISI 440C was in accordance with that reported by in [7].

The resulting microstructures after the heat treatments for AISI 420 samples are shown in Figs. 1*a*, *b*, respectively. The samples exhibited a large number of secondary carbides embedded in a martensitic matrix. The application of the cryogenic treatment resulted in the reduction of the average carbide size and a more uniform spatial distribution. The slight hardness increase (Table 2) in DCT samples was attributed to the modifications of the carbide precipitates [5]. Additionally, we hypothesize that the reduction of the carbide volume fraction that changed from 16.8% in CHT samples to 11.9% in DCT implied that the martensitic matrix of DCT samples had a higher degree of carbon saturation, and therefore an increased hardness.

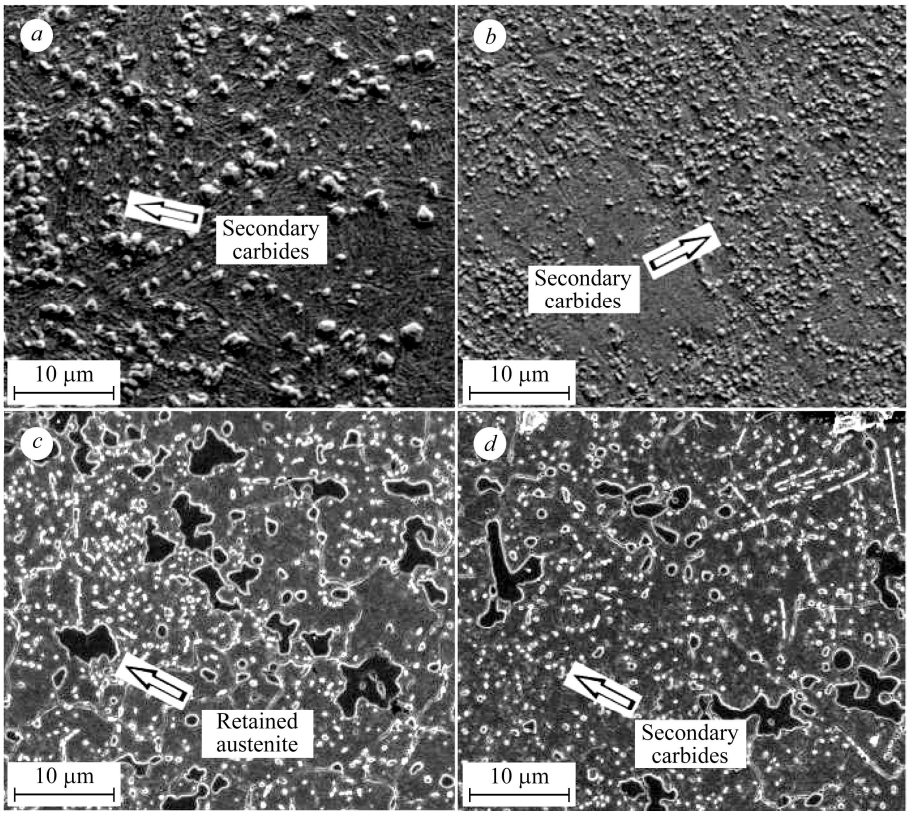

Fig. 1. SEM images: *a* – AISI 420 CHT; *b* – AISI 420 DCT; *c* – AISI 440C CHT; *d* – AISI 440C DCT samples.

It should be noted that the AISI 420 steel rebar used for obtaining the samples has a rather low carbon content (0.17 wt.%), which improved its hardenability due to a reduction in the probability of cracking during cooling. This ensured minimal content of retained austenite into both CHT and DCT samples. From the absence of austenitic peaks at the diagrams of XRD analysis (Fig. 2*a*), it is estimated that the volume of retained austenite is below 3%, which is the detection limit of the diffractometer. Similar results were informed in [18, 19].

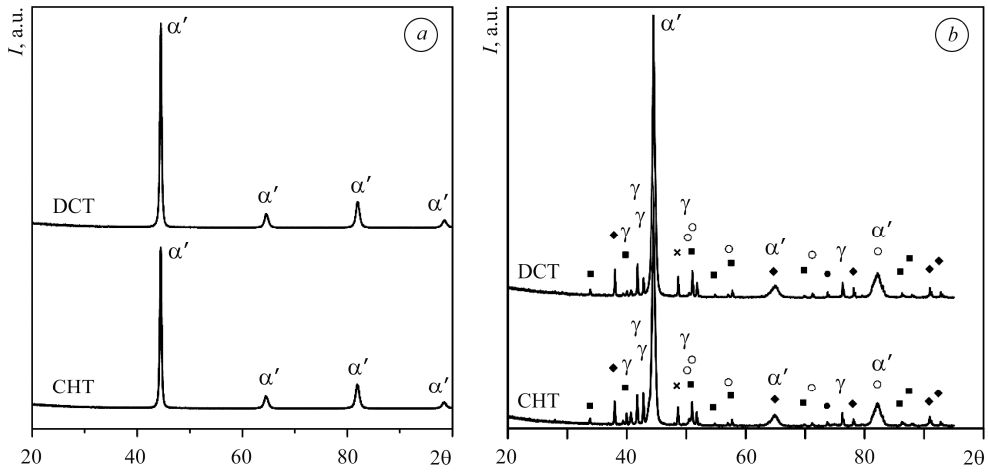

Fig. 2. XRD spectra: *a* – AISI 420; *b* – AISI 440C samples: ◆ – MC; ■ – MC_6C; ○ – M_7C_3; ● – $M_{23}C_6$; × – Cr_3C_2).

In the case of AISI 440C, the microstructures of the samples are more complex, as can be seen in Fig. 1*c*, *d*, respectively, consisting of a mixture of primary and secondary carbides [20], islands of retained austenite and the martensitic matrix. These microstructures are consistent with those reported in [21–24]. The XRD analysis (Fig. 2*b*), confirmed that the application of the cryogenic treatment reduced the intensity of the austenite peaks. It should be noted that it was not possible to find the XRD spectra of the AISI 440C steel treated cryogenically in the open literature.

The quantitative analysis of the microstructural images obtained by SEM indicated a decrease in the amount of retained austenite by 50% (Table 2), which contributed to the hardness increase of the AISI 440-DCT samples. No significant differences between the carbide precipates of the AISI 440C samples were found. The microstructural characterization using image analysis was performed as follows. First, images at magnification of ×5000 were taken at the same positions using both secondary (SE) and backscattered electrons (BSE). This enabled the manual identification and measurement using FIJI of the retained austenite regions, as pictured in the highlighted contour in Fig. 3*a*. These regions show no contrast against the martensitic matrix and therefore appear as black zones in the BSE images (Figs. 3*a*, *b*). Afterward, the BSE image was converted to binary mode (Fig. 3*c*), in which carbides appeared as white regions. Finally, the particle count plugin of the software was used for determining the amount and size of the carbides (Fig. 3*d*). The software created a mask, showing the regions being considered as particles (i.e. carbides) and a numerical result, indicating the size in pixels of every detection. The total areas of the zones identified in the analyzed image as corresponding to residual austenite or carbides were divided by the total area of the image to estimate the respective volume fractions. This procedure was repeated in 10 images for every specimen type.

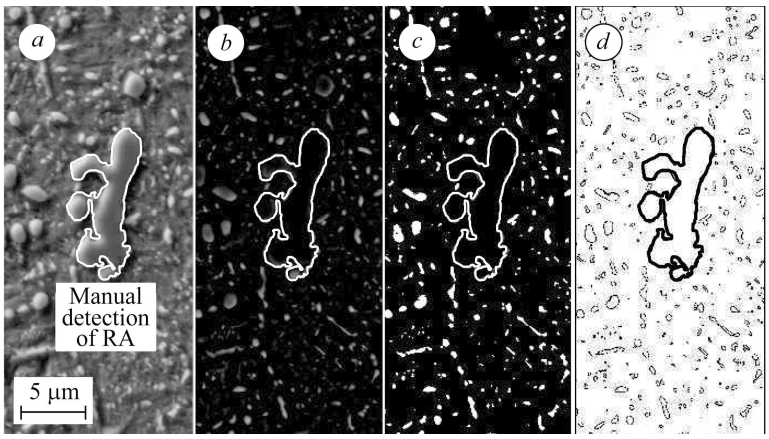

Fig. 3. Image analysis procedure using FIJI and particle count plugin for microstructural characterization.

Table 2. Hardness and microstructural features overview

Sample	Vickers hardness, $HV_{0.5}$	Retained austenite	Volume fraction of carbides	Carbide mean diameter, μm
		%		
420-CHT	560 ± 27	< 3.0	16.8 ± 0.1	0.87 ± 0.31
420-DCT	586 ± 24	< 3.0	11.9 ± 0.3	0.33 ± 0.07
440-CHT	660 ± 23	10.4 ± 1.1	4.5 ± 1.3	0.38 ± 0.15
440-DCT	712 ± 35	5.1 ± 0.7	4.2 ± 0.9	0.38 ± 0.11

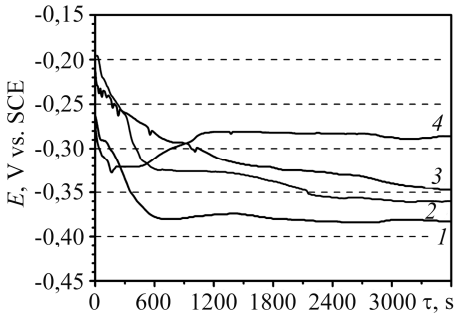

Fig. 4. OCP vs. time plot in an aerated 0.5 M NaCl solution for: *1* – 420-CHT; *2* – 420-DCT; *3* – 440-CHT; *4* – 440-DCT samples.

Electrochemical experiments. Fig. 4 shows the OCP variations with time in an aerated 0.5 M NaCl solution. In the case of both the 420-CHT and DCT specimens, the OCP values present a similar decrease with time due to dissolution of the passive film as was previously suggested [16]. On the other hand, the OCP value for 420-DCT sample does not show a significant difference to the OCP value of the 420-CHT sample after 1 h of immersion in the chloride solution (only +23 mV). Moreover, when the OCP variation was analyzed over time for the AISI 440C samples, it was observed that at the beginning of the experiment (during the first 1000 s) the 440-CHT samples had a more positive OCP value than the 440-DCT and then its value became lower to compare to the 440-CHT. It is possible that the increase in the OCP value observed after 500 s of immersion for the 440-DCT sample is due to the formation of corrosion products that gives the substrate a certain degree of passivity in chloride solution.

The cyclic polarization curves and the potentiostatic response for the differently treated samples in an aerated 0.5 M NaCl solution are shown in Fig. 5. All the samples show an active corrosion behavior controlled by the resistance of the solution at noble potentials, in which the corrosion rate is controlled by the transportation of cathodic species.

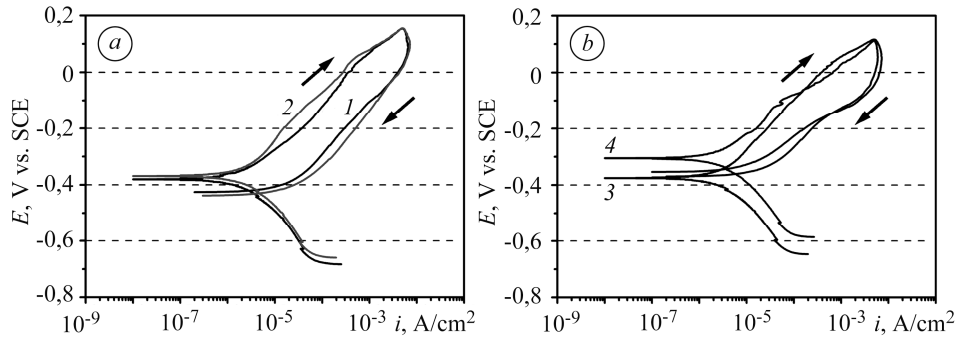

Fig. 5. Single-cycle anodic polarization scans (1 mV·s^{-1}) in an aerated 0.5 M NaCl solution for: *1* – 420-CHT; *2* – 420-DCT; *3* – 440-CHT; *4* – 440-DCT samples. The arrows indicate the scan direction.

No significant differences were observed between the polarization curves of 420-CHT and 420-DCT samples (Fig. 5*a*), including the shape of the curve, the corrosion potential, the pitting potential, the repassivation potential, and the magnitude of the current density. However, in the last case, the hysteresis was a little higher. In both cases, the repassivation potential is lower than the corrosion potential, which indicates that the 420-CHT and 420-DCT samples will remain in an active state once their passivity is destroyed, allowing the pits to grow without interruption.

On the other hand, considering the AISI 440C samples, it can be said that the 440-CHT sample shows a less noble corrosion potential than the 440-DCT one (Fig. 5*b*), as was previously mentioned. Besides, only the 440-CHT sample has a repassivation potential higher than its corrosion potential, which indicates that this type of sample can regenerate its passivation layer in the event of a rupture. On the contrary, the cryo-

genic treatment modifies this self-repairing property when the passive film is damaged, since its repassivation potential is lower than its corrosion potential.

In order to check the pitting corrosion resistance under more drastic conditions, the current density-time response was registered for the different treated samples in the aerated 0.5 M NaCl solution at a potential in which pits appear on the entire surface (0.20 V (SCE)) (Figs. 6*a*, *b*). The current (*i*) versus time (τ) profiles for the 420-CHT and 420-DCT samples are very similar, which means that the cryogenic treatment does not modify the degree of pitting corrosion protection observed in the sample subjected to a conventional heat treatment (Fig. 6*a*). Nevertheless, the current density measured for the 440-CHT sample is lower than for the 440-DCT sample (Fig. 6*b*), which indicates that the cryogenic treatment considerably reduces the pitting corrosion resistance of the material. The main objective of this evaluation is to assess the corrosion resistance of the materials under service conditions, where the surfaces of the components are covered with passivating films. The evaluation of the corrosion resistance of the base material requires corrosive environments that remove such passivating films [25] being the subject of our future research.

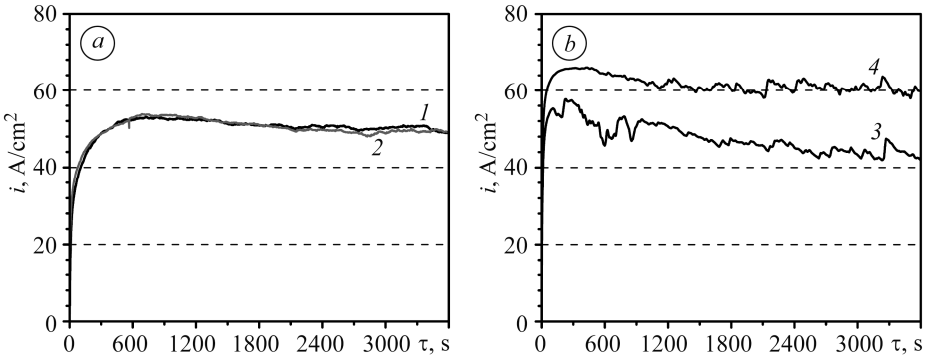

Fig. 6. Potentiostatic response obtained at 0.20 V (SCE) in the aerated 0.5 M NaCl solution for: *1* – 420-CHT; *2* – 420-DCT; *3* – 440-CHT; *4* – 440-DCT samples.

The above results could be explained by considering the amount of retained austenite after thermal treatment carried out, either conventionally or cryogenically. As was previously postulated [16], the amount of retained austenite has a critical role in determining the pitting corrosion resistance of the AISI 420 steel. These authors have found that the pitting corrosion resistance increases with the amount of retained austenite. Authors [26] obtained similar conclusions when working with the AISI 440C steel. However, the processing method used in [26] (laser melting) is very different from the one used in this present study. To the best of our knowledge, there are no published results in the open literature on the corrosion resistance of the cryogenically treated AISI 440C steel.

As it was aforementioned, the AISI 420 steel used in this study had a low carbon content, which in turn resulted in very low amounts of retained austenite (less than 3% in both groups of samples, see Table 2), even in the quenched and tempered condition. Due to this characteristic, there is no significant difference between the corrosion resistances of the AISI 420 samples. Our results show that modifications in the carbide size and distribution have no significant influence on the corrosion resistance of the steel. It should be noted that although Wang and collaborators reached similar results [16], they did not quantified the modifications in carbide distribution due to the application of cryogenic treatments.

In the case of the AISI 440C samples, the application of the cryogenic treatment reduced the content of retained austenite by almost 50%. This result was expected as this steel had a relatively high martensite finish temperature (MF) due to its elevated

carbon content. In those cases, the cryogenic cooling stage contributes to the transformation of the retained austenite into martensite, being the main reason why the 440-DCT sample has a lower pitting corrosion resistance than the 440-CHT sample.

Corrosion damage evaluation. Fig. 7 shows the corrosion damage of the AISI 420 samples, where it can be seen that pits develop in the surroundings of carbides and progress into the matrix. The pits were uniformly distributed over the exposed area of the samples. This is an expected phenomenon, as carbides have a different electrode potential than the metallic matrix, giving place to galvanic processes in the presence of electrolyte [27]. However, there seems to be a competence between two mechanisms: the first one is associated with a decrease in the volume fraction of carbides shown by the 420-DCT samples (see Table 2), which impacts positively on the corrosion resistance of the material, and the second one with an increase in the number of carbides (Fig. 1*b*). This should promote a higher amount of pit initiation sites, but as carbides in the 420-DCT are smaller, both effects neutralize each other and the corrosion resistance of the AISI 420 is therefore not affected by the application of the cryogenic treatment.

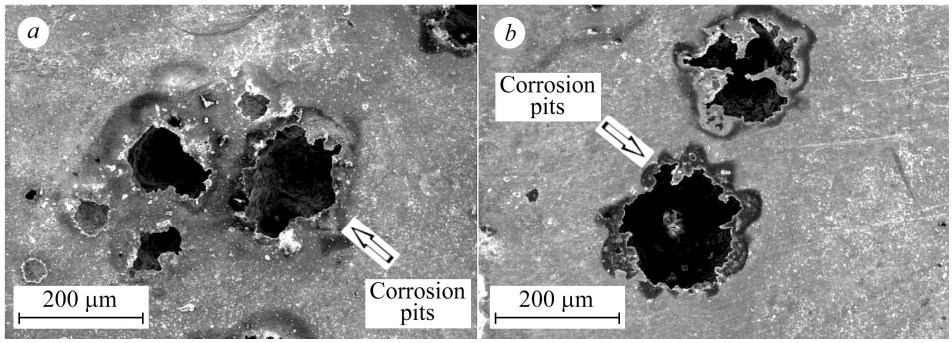

Fig. 7. SEM micrographs of corrosion pits in: *a* – 420-CHT; *b* – 420-DCT samples.

The chemical characterization of the corroded surfaces using SEM-EDS (Fig. 8) showed a higher concentration of oxygen inside the pits. The semi-quantitative analysis in Zone 1 yielded 23.75 at.% of oxygen, while in Zone 2 it was 1.26 at.%. This was an expected result as the corrosion process was heavily localized in the pits. It is speculated that the corrosion products are a mixture of chromium and iron oxides and hydroxides, as described [28].

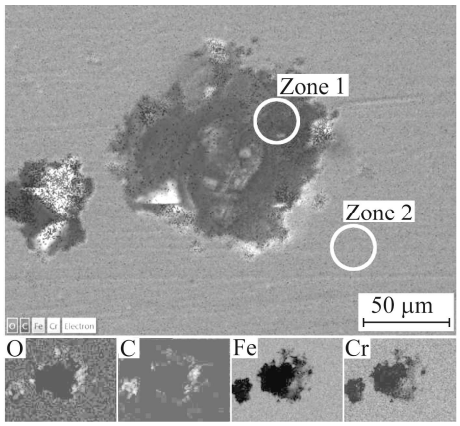

Fig. 8. EDS Mapping of a corrosion pit in the 420-DCT specimen.

In the case of the AISI 440C samples (Fig. 9), the corrosion damage is more extensive, showing pits and intergranular corrosion (see Fig. 10), in accordance with the

behavior seen in the potentiodynamic experiments in Fig. 5*b*. These results are consistent with the high carbon content of the material that reduces significantly its corrosion resistance compared to steels with lower quantities of carbon [29].

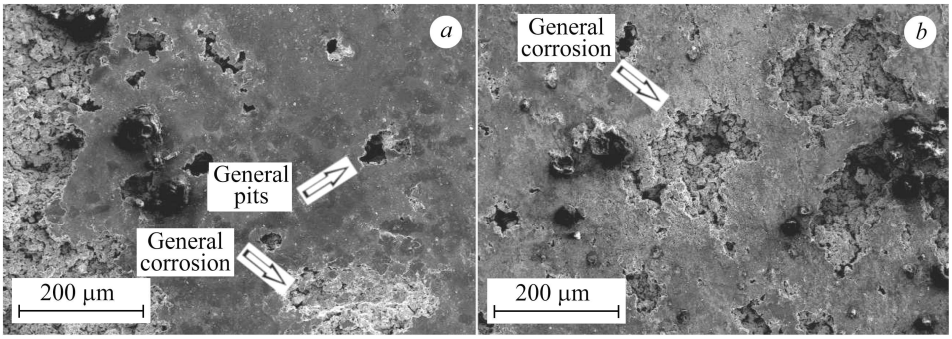

Fig. 9. SEM micrographs of the corrosion damage in: *a* – CHT; *b* – DCT AISI 440C samples.

Fig. 10. Intergranular corrosion damage in the 440-DCT sample.

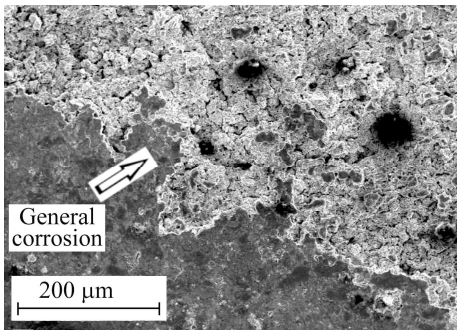

A closer examination of the chemical composition in the corrosion pit surroundings is presented in Fig. 11. The oxygen content in Zone 1 was 33.12 at.%, while in Zone 2 it was 8.60 at.%, thus signaling a highly localized corrosion process. Besides, the oxygen levels outside the pitted regions of the AISI 440C (~ 8.60 at.%) samples were higher on average than those measured in the AISI 420 samples (~1.30 at.%).

The EDS analysis of the region with general corrosion in the 440-DCT sample is shown in Fig. 12, where it can be seen that the oxygen distribution is rather homogeneous in both the original surface (Zone 2) of the sample and inside the heavily dissolved region (Zone 1). The oxygen content in Zone 1 was 18.51 at.%, while in Zone 2 it was 18.65 at.%.

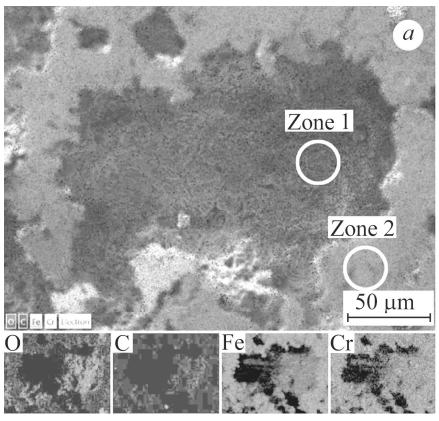

Fig. 11.

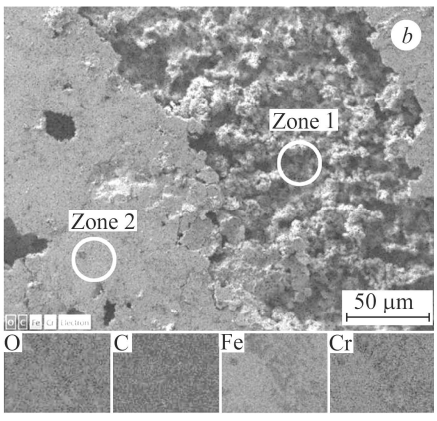

Fig. 12.

Fig. 11. EDS mapping of corrosion pit in the 440-DCT sample.

Fig. 12. EDS mapping of a region showing intergranular corrosion in the 440-DCT sample.

CONCLUSIONS

Based on the results obtained from the study of the electrochemical behavior of two cryogenically treated martensitic stainless steels, the following conclusions have been drawn. In martensitic stainless steels with relatively low carbon content, such as AISI 420, cryogenic treatments generate a reduction in the average carbide size (0.87 vs. 0.33 μm) that enhances the hardness of the material, without the negative affect of neither its pitting resistance nor its repassivation potential. On the other hand, the main effect of the application of the cryogenic treatment on AISI 440C is the reduction in the content of retained austenite, which is from 10.4 to 5.1% in the 440-DCT samples. In this case, the hardness of the cryogenically treated material improves, but at the expense of its corrosion resistance. In particular, the pitting resistance of the cryogenically treated AISI 440 samples was significantly reduced as well as its repassivation capacity. The obtained results highlight the importance of carefully designing cryogenic treatments for martensitic stainless steels to generate a proper balance between mechanical properties and corrosion resistance.

Acknowledgments. The authors wish to express their appreciation for the funding given by the Secretaría de Ciencia y Técnica – UNS (PGI 24/M146), the Consejo Nacional de Investigaciones Científicas y Técnicas (CONICET – PIP 112–20150 – 100147) and the Agencia Nacional de Promoción Científica y Tecnológica (ANPCYT PICT-2015-0726 and PICT 2013-0616).

1. *Vojteh Leskovšek B. P. and Ule B.* Influence of deep cryogenic treatment on microstructure, mechanical properties and dimensional changes of vacuum heat-treated high-speed steel // Heat Treat. Met. – 2002. – **29**, № 3. – P. 72–76.
2. *Leskovsek V. M. and Kalin J. V.* Influence of deep-cryogenic treatment on wear resistance of vacuum heat-treated HSS // Vacuum. – 2006. – **80**. – P. 507–518.
3. *Deep* cryogenic treatment of tool steels / B. Podgornik, I. Paulin, B. Zajec, S. Jacobson, and V. Leskovšek // J. Mat. Proc. Techn. – 2016. – **229**. – P. 398–406.
4. *Pellizzari M. and Molinari A.* Deep cryogenic treatment of cold work tool steel // Proc. of 6th Int. Tooling Conf. – 2002. – P. 657–669.
5. *Prieto G., Perez Ipiña J. E., and Tuckart W. R.* Cryogenic treatments on AISI 420 stainless steel: microstructure and mechanical properties // Mat. Sci. Eng. A. – 2014. – **605**. – P. 236–243.
6. *Prieto G., Tuckart W. R., and Perez Ipiña J. E.* Influence of a cryogenic treatment on the fracture toughness of an AISI 420 martensitic stainless steel // Mat. Tehn. – 2017. – **4**, № 51.
7. *Idayan A., Gnanavelbabu A., and Rajkumar K.* Influence of deep cryogenic treatment on the mechanical properties of AISI 440C bearing steel // Proc. Eng. – 2014.
8. *Koneshlou M., Meshinchi Asl K., and Khomamizadeh F.* Effect of cryogenic treatment on microstructure, mechanical and wear behaviors of AISI H13 hot work tool steel // Cryogenics (Guildf). – 2011. – **51**, № 1. – P. 55–61.
9. *Effect* of cryogenic treatment and aging treatment on the tensile properties and microstructure of Ti–6Al–4V alloy / K. Gu, H. Zhang, B. Zhao, J. Wang, Y. Zhou, and Z. Li // Mat. Sci. Eng. A. – 2013. – **584**. – P. 170–176.
10. *Enhancing* wear resistance of Mg–Zn–Gd alloy by cryogenic treatment / Y. Liu, S. Shao, C. Xu, X. Yang, and D. Lu // Mat. Lett. – 2012. – **76**. – P. 201–204.
11. *Wear* of cryo-treated engineering polymers and composites / J. Indumathi, J. Bijwe, A. K. Ghosh, M. Fahim, and N. Krishnaraj // Wear. – 1999. – **225**. – P. 343–353.
12. *Low-temperature* martensitic transformation and deep cryogenic treatment of a tool steel / A. I. Tyshchenko, W. Theisen, A. Oppenkowski, S. Siebert, O. N. Razumov, A. P. Skoblik, V. A. Sirosh, Y. N. Petrov, and V. G. Gavriljuk // Mat. Sci. Eng. – 2010. – **527**. – P. 7027–7039.
13. *Das D., Dutta A. K., and Ray K. K.* Optimization of the duration of cryogenic processing to maximize wear resistance of AISI D2 steel // Cryogenics (Guildf). – 2009. – **49**, № 5. – P. 176–184.

14. *Enhancing* the wear resistance of case carburized steel (En 353) by cryogenic treatment / A. Bensely, A. Prabhakaran, D. Mohan Lal, and G. Nagarajan // Cryogenics (Guildf). – 2005. – **45**, № 12. – P. 747–754.
15. *Никифорчин Г. М., Ткачук Ю. М., Студент О. З.* Експлуатаційна деградація сталі 20Х13 лопаток парових турбін ТЕС // Фіз.-хім. механіка матеріалів. – 2011. – **47**, № 4. – С. 28–35.
(*Nykyforchyn H. M., Tkachuk Y. M., and Student O. Z.* In-service degradation of 20Kh13 steel for blades of steam turbines of thermal power plants // Materials Science. – 2012. – **47**, № 4. – P. 447–456.)
16. *Corrosion* behavior of deep cryogenically treated AISI 420 and AISI 52100 steel / W. Wang, V. Srinivasan, S. Siva, A. Bensely, M. Lal, and A. Alfantazi // Corrosion. – 2014. – **9312**. – P. 708–720.
17. *Fiji:* an open-source platform for biological-image analysis / J. Schindelin, I. Arganda-Carreras, E. Frise, V. Kaynig, M. Longair, T. Pietzsch, S. Preibisch, C. Rueden, S. Saalfeld, and B. Schmid // Nat. Methods. – 2012. – **9**, № 7. – P. 676–682.
18. *Dodds S., Jones A. H., and Cater S.* Tribological enhancement of AISI 420 martensitic stainless steel through friction-stir processing // Wear. – 2013. – **302**, № 1–2. – P. 863–877.
19. *Microstructure* and hardness characterisation of laser coatings produced with a mixture of AISI 420 stainless steel and Fe–C–Cr–Nb–B–Mo steel alloy powders / S. Da Sun, D. Fabijanic, A. Ghaderi, M. Leary, J. Toton, S. Sun, M. Brandt, and M. Easton // Surf. Coat. Techn. – 2016. – **296**. – P. 76–87.
20. *Standard* practice for X-ray determination of retained austenite in steel with near random crystallographic orientation 1. – Astm, 03(Reapproved 2008). – 2009. – P. 1–7.
21. *Puli R. and Janaki Ram G. D.* Microstructures and properties of friction surfaced coatings in AISI 440C martensitic stainless steel // Surf. Coat. Techn. – 2012. – **207**. – P. 310–318.
22. *Yang J. R., Yu T. H., and Wang C. H.* Martensitic transformations in AISI 440C stainless steel // Mat. Sci. Eng. A. – 2006. – **438**–**440**(December 2005). – P. 276–280.
23. *Microstructure* and mechanical properties of 0.63c–12.7cr martensitic stainless steel during various tempering treatments // Mat. Manuf. Proc. – 2010. – **25**, № 4. – P. 246–248.
24. *Investigation* of microstructures and properties of 440C martensitic stainless steel / S. H. Salleh, M. Z. Omar, J. Syarif, M. J. Ghazali, S. Abdullah, and Z. Sajuri // Int. J. Mech. Mat. Eng. – 2009. – **4**, № 2. – P. 123–126.
25. *Звірко О. І.* Електрохімічні методи оцінювання деградації конструкційних сталей тривалої експлуатації // Фіз.-хім. механіка матеріалів. – 2016. – **52**, № 4. – С. 126–131.
(*Zvirko O. I.* Electrochemical methods for the evaluation of the degradation of structural steels intended for long-term operation // Materials Science. – 2017. – **52**, № 4. – P. 588–594.)
26. *Effect* of processing conditions on the corrosion performance of laser surface-melted AISI 440C martensitic stainless steel / C. T. Kwok, K. H. Lo, F. T. Cheng, and H. C. Man // Surf. Coat. Techn. – 2003. – **166**, № 2–3. – P. 221–230.
27. *Alrubaiey S. I. and Hasan S. F.* Prediction the initiation of pitting corrosion depending on carbides in the microstructure of 304 stainless steel // Eng. Techn. J. – 2017. – **35**, № 10. – P. 975–980.
28. *Characterization* of corrosion scale formed on stainless steel delivery pipe for reclaimed water treatment / Y. Cui, S. Liu, K. Smith, K. Yu, H. Hu, W. Jiang, and Y. Li // Water Res. – 2016. – **88**(November). – P. 816–825.
29. *Dománková M., Kocsisová E., and Slatkovský I.* The microstructure evolution and its effect on corrosion properties of 18Cr–12Ni–2, 5 Mo steel annealed at 500...900°C. – 2014. – **11**, № 3. – P. 125–137.

Received 22.12.2020